Geology

Normal Faulting and Evolution of Fluid Discharge in a Jurassic Seafloor Ultramafic-Hosted Hydrothermal System

--Manuscript Draft--

Manuscript Number:	
Full Title:	Normal Faulting and Evolution of Fluid Discharge in a Jurassic Seafloor Ultramafic-Hosted Hydrothermal System
Short Title:	Evolution of Fluid Discharge
Article Type:	Article
Keywords:	hydrothermal systems, sulfide mineralization, marine geology, geochemistry, faults, mid ocean ridges
Corresponding Author:	Jeffrey Alt University of Michigan Ann Arbor, MI UNITED STATES
Corresponding Author Secondary Information:	
Corresponding Author's Institution:	University of Michigan
Corresponding Author's Secondary Institution:	
First Author:	Jeffrey Alt
First Author Secondary Information:	
Order of Authors:	Jeffrey Alt
	Laura Crispini
	Laura Gaggero
	David Levine
	Giorgia Lavagnino
	Wayne Shanks
	Cayce Gulbransen
Order of Authors Secondary Information:	
Manuscript Region of Origin:	ITALY
Abstract:	We document a normal fault that lies at a high angle to an oceanic detachment that exposed peridotite on the Jurassic seafloor. Such faults are inferred to be discharge zones for ultramafic-hosted hydrothermal systems, but have not yet been sampled from the modern seafloor. The fault comprises 0.5-2 m thick zones of sheared talc + sulfide within serpentinite, and ends upward in carbonated serpentinite, massive sulfide and pillow basalts. Talc alteration, enrichment in metals, LREE, and 34S of the fault rocks provide evidence of a conduit for discharge of high-temperature hydrothermal fluids related to fluid circulation and mineralization. At the seafloor, the fault rocks have been replaced by later Fe-dolomite + minor quartz, chlorite and sulfides at temperatures of 90-120˚C during waning hydrothermal activity. This is the first view of the subsurface discharge zone of a seafloor ultramafic-hosted hydrothermal system, showing that normal faults provide pathways to focus fluid flow and reaction. An important new result is field and geochemical evidence that high temperature hydrothermal systems with black smoker-type venting, sulfide mineralization and talc alteration can evolve to lower temperature Lost City-type venting and carbonate mineralization.
Suggested Reviewers:	Freder Klein fklein@whoi.edu

	Muriel andreani muriel.andreani@univ-lyon1.fr
	Sven Petersen spetersen@geomar.de
	Dionysis Foustoukos dfoustoukos@carnegiescience.edu

Normal Faulting and Evolution of Fluid Discharge in a Jurassic Seafloor Ultramafic-Hosted Hydrothermal System

Jeff Alt[1], Laura Crispini[2], Laura Gaggero[2], David Levine[1], Giorgia Lavagnino[2], Pat Shanks[3], and Cayce Gulbransen[3]

[1]Earth and Environmental Sciences, University of Michigan, Ann Arbor, MI, USA

[2]DISTAV, University of Genova, Corso Europa 26, 16132 Genova, Italy

[3]U.S. Geological Survey, 973 Denver Federal Center, Denver, CO, USA

Published in Geology (2018) 46 (6): 523–526 https://doi.org/10.1130/G40287.1

ABSTRACT

We document a normal fault that lies at a high angle to an oceanic detachment that exposed peridotite on the Jurassic seafloor. Such faults are inferred to be discharge zones for ultramafic-hosted hydrothermal systems, but have not yet been sampled from the modern seafloor. The fault comprises 0.5-2 m thick zones of sheared talc + sulfide within serpentinite, and ends upward in carbonated serpentinite, massive sulfide and pillow basalts. Talc alteration, enrichment in metals, LREE, and ^{34}S of the fault rocks provide evidence of a conduit for discharge of high-temperature hydrothermal fluids related to fluid circulation and mineralization. At the seafloor, the fault rocks have been replaced by later Fe-dolomite + minor quartz, chlorite and sulfides at temperatures of 90-120˚C during waning hydrothermal activity. This is the first view of the subsurface discharge zone of a seafloor ultramafic-hosted hydrothermal system, showing that normal faults provide pathways to focus fluid flow and reaction. An important new result is field and geochemical evidence that high temperature hydrothermal systems with black

smoker-type venting, sulfide mineralization and talc alteration can evolve to lower temperature Lost City-type venting and carbonate mineralization.

I. INTRODUCTION

Detachment faults at slow-spreading mid-ocean ridges expose mantle peridotite on the seafloor, leading to serpentinization of peridotite, which is important for elemental exchange with seawater, supports microbial life, and contributes to cycling of water and elements in subduction zones (Alt and Shanks, 1998, 2003; Deschamps et al., 2010). Serpentinization can occur over a range of temperatures, from bottom seawater temperatures (near 0˚C) up to ~350˚C in high temperature ultramafic-hosted hosted hydrothermal systems. The latter are driven by heat from gabbroic intrusions and result in black-smoker-type hydrothermal fluids forming metal sulfide deposits where they vent at the seafloor (Petersen et al., 2009; Schmidt et al., 2007). Detachment faults can focus high-temperature hydrothermal fluid flow at depth, (McCaig et al., 2007), but where black smoker vents and sulfide mineralization lie directly atop the exposed footwall peridotite, the discharge zones are inferred to be normal faults at high angle to the detachment surface (Fig. 1; Petersen et al., 2009; Andreani et al., 2014). Such faults are observed on seismic reflection profiles (Tucholke et al., 2008), and seismic data reveal a normal fault at the Logatchev hydrothermal field on the MAR, dipping toward the spreading axis and bottoming out in basaltic magma 5 km below the seafloor (Andersen et al., 2015). At the Lost City vent field, alignment of vents and carbonate deposits at the surface indicate a normal fault that focuses lower-temperature hydrothermal upflow (Denney et al., 2016). Little direct evidence is available about the nature of the fault zones and their effects on fluid flow and serpentinization in the subsurface of the modern seafloor, but study of ancient oceanic basement can provide meaningful insights.

II. STUDY AREA

The northern Apennine ophiolites are fragments of Jurassic oceanic crust that formed at slow or ultra-slow spreading centers, on the oceanward side of an ocean–continent transition (Principi et al., 2004; Marroni and Pandolfi, 2007). Peridotites are clinopyroxene-poor depleted spinel lherzolites and harzburgites, having $^{87}Sr/^{86}Sr$ ratios like MORB mantle (~0.7022; Rampone et al., 1998). High $^{143}Nd/^{144}Nd$ ratios and Nd model ages of 275 Ma indicate depletion of subcontinental mantle during Permian extension (Rampone et al., 1998). At ~165 Ma the peridotites were intruded by MORB gabbros, exposed on the Tethyan seafloor by detachment faulting, and covered by MORB lavas and pelagic chert and limestone (Marroni and Pandolfi, 2007).

Figure 2 shows part of a 35 km^2 ophiolite body, with the base of the pillow lavas marking the detachment surface. The sediments dip ~25˚ to the north, enabling use of topography (Table S1) to estimate depths beneath the paleo-seafloor as defined by the base of the sediment. In this area we discovered fault zones in serpentinized peridotite that extend more than 300 m below the paleo-seafloor, and that are associated with sulfide deposits similar to those atop ultramafic rocks on the modern seafloor (Fig. 2; Garuti et al 2008).

III. METHODS

Mineralogy and petrographic relationships were determined by optical microscopy. Analytical techniques and data for bulk rock major and trace elements and carbon and sulfur isotope compositions, along with carbon, oxygen, and sulfur isotope compositions of secondary minerals are given in Tables S1 - S3 in the Supplementary Data.

IV. RESULTS AND DISCUSSION

A. Background Serpentinite

Two peridotite samples 440-600 m from the oceanic fault and 450-540 m below the paleo-seafloor (Fig. 2) are completely serpentinized, with mesh, ribbon and bastite textures (Fig. S1). Cr spinel is present as up to 300 μm irregular globular grains typical of resorbed textures. Magnetite is common as 1-5 μm grains in mesh-forming serpentine veins, and as larger aggregates in later cross-cutting serpentine veins. Minor pentlandite is present as 2-20 μm grains disseminated in serpentine mesh and bastite (Fig. S1).

The serpentinites have slightly low MgO/SiO_2 ratios compared to terrestrial peridotite and lack brucite, similar to many seafloor serpentinites, which can be attributed to alteration by a seawater fluid enriched in silica (Malvoisin, 2015). The rocks exhibit LREE depletion trends like fresh peridotite (Fig 3), but positive correlations between LREE and HFSE (e.g., Nb vs La, Th vs Ce) suggest the effects of melt percolation (Niu, 2004). The lack of significant chemical changes during serpentinization indicates reaction at low water/rock ratios. O and H isotope data for nearby serpentinites indicate temperatures of ~240˚C and hydrothermal fluids enriched in ^{18}O (Barrett and Friedrichsen, 1989). The presence of pentlandite and absence of reduced, low-S phases (awaruite, heazelwoodite) indicate relatively high sulfur activity (Foustoukos et al., 2015)

B. Talc-Rich Fault Zone

In the central part of this area (Fig. 2) the fault outcrops as 0.5 to 2 m wide sheared talc + sulfide, the latter now mostly weathered to red Fe-oxides. Major structures include an antiform plunging to the southwest, and a subvertical shear zone trending N-S that is cut by the antiform (Fig. 2B). The fault pinches and swells, and has numerous splays. Some kinematic indicators show movement like that at the paleo-seafloor to the west (with the eastern hanging wall moving downward to the south), but other motions are also indicated and absolute motion is uncertain.

The fault rocks consist of massive fine-grained talc, but talc pseudomorphs of mesh textured serpentinite are common (Fig. S2), indicating a replacement origin for much of the talc. Deformation within the fault zone is thus not pervasive, with anastomosing shear bands within talc-altered serpentinite. Also present are local disseminated 1-2 μm sulfide grains (pentlandite, pyrrhotite, chalcopyrite and sphalerite) and 2-120 μm grains and aggregates of magnetite, all partly replaced by weathering products (hematite and Fe-oxyhydroxide). The fault rocks have elevated SiO_2 and low MgO contents (58 and 25-26 wt%, respectively), and are enriched in Fe, Cu, and Zn (Fig. 5, Table S1). The chemical changes are consistent with silica metasomatism, metal deposition, and leaching of Mg by high-temperature (~350˚C) silica- and metal-rich hydrothermal fluids upwelling along the fault (Schmidt et al., 2007). Breakdown of olivine and Cr spinel led to losses of Ni and Cr from the fault rocks to hydrothermal fluids. HREE depletion and LREE enrichment of the fault rocks are consistent with fluids sampled from modern seafloor ultramafic hosted hydrothermal systems (Fig. 3). Sulfides are mostly oxidized in outcrop, but one sample from 300 m below the paleo-seafloor consists of talc and sulfides replacing serpentine. The presence of pyrite with pyrrhotite and chalcopyrite indicates relatively high f_{O_2} and/or sulfur activity compared to fluids venting from modern ultramafic-hosted hydrothermal systems (Fig. S2; Alt and Shanks, 2003; Foustoukos et al., 2015). Pyrite from this rock has $\delta^{34}S$ = 5.7‰; Table S2), similar to values for massive sulfide deposits overlying the fault (mean = +6.7‰; Garuti et al., 2009) and to sulfide in hydrothermal deposits from seafloor ultramafic settings (Rouxel et al., 2004), providing further evidence for discharging high-T hydrothermal fluids in the fault zone.

C. Carbonated Fault Zone at the Seafloor

At the paleo-seafloor on the west side of the field area (Fig. 2) the fault is 4 m wide, outcropping for over 250 m and oriented at a high angle to the paleo-seafloor. Here it is clearly a normal fault juxtaposing serpentinite breccia and serpentinite on the west against pillow basalts on the east, and ending upward in massive sulfide and hydrothermally altered pillow lavas overlain by pelagic chert and limestone (Fig. 4A). Lenses of sheared and chloritized basalt locally border the fault.

The normal fault zone comprises >90% Fe-dolomite (Table S3) with minor quartz, calcite, chlorite, serpentine, sulfides and chrome spinel (Fig 4B). Pyrite, pyrrhotite, pentlandite, minor chalcopyrite, and trace sphalerite are present as 5-80 μm grains and up to 350 μm aggregates. Trace Cr spinel has a morphology like that in the serpentinites, but the globular grains are fragmented and bordered by magnetite replacement rims (Fig. 4C). Magnetite is otherwise absent in these rocks.

Compared to the background serpentinites, the near-seafloor fault rocks are enriched in metals (Fe, Mn, Cu, Zn), and have low SiO_2 and very low MgO contents (Fig. 4; Table S1). They are also enriched in Sr, Y, and REE, especially the LREE (Fig. 3). The setting of the fault, ending upward in massive sulfide, indicates that the fault was the conduit for discharging hydrothermal fluids, and the chemistry of the fault rocks is consistent with high-temperature black smoker type fluids, enriched in metals and LREE (Douville et al., 2002; Schmidt et al., 2007). The sulfide mineral assemblage indicates relatively high f_{O_2} and sulfur activity (Foustoukos et al., 2015). The high Cr contents of the fault rocks and the presence of relict Cr spinel show that the fault rocks are largely the result of replacement of serpentinized peridotite, with the low Mg contents resulting from leaching by Mg-depleted hydrothermal fluids (Douville et al., 2002; Schmidt et al., 2007). The host serpentinite breccias and serpentinite are veined by and variably altered to talc, consistent with interaction of serpentinite with high-temperature (~350˚C) silica-rich, Mg-poor black-smoker-like hydrothermal fluids. Talc veins in these rocks are cut by calcite veins, indicating that carbonation followed high temperature hydrothermal discharge.

The high Ca, Sr, and CO_2 contents of the near-seafloor fault rocks reflect carbonation of serpentinite (Fig. 5; Table S1). Carbonate in the fault rocks has $\delta^{18}O$ values of 19.8-20.9‰, indicating temperatures of 90-120˚C if formed in equilibrium with seawater or hydrothermal fluids (0 to +2‰; Vasconcelos et al., 2005; Table S2). This is consistent with carbonation of the fault rocks during waning hydrothermal activity, as cooling fluids become more alkaline (Foustoukos et al., 2008). Carbonate drilled from the fault rocks has $\delta^{13}C$ values of -0.8 to -1.5‰ VPDB and bulk rocks have values of -1.8 to -2.3‰. The $\delta^{13}C$ values are consistent with incorporation of carbon from oxidation of reduced carbon species in hydrothermal fluids during mixing with seawater, like at Lost City (Fruh-Green et al., 2003). The carbonate-rich mineral assemblage of the fault rocks is similar to that predicted by thermodynamic modeling of serpentinite reacting with CO_2-enriched seawater fluids (Klein and Garrido, 2011).

The presence of sphalerite and Zn enrichments in the fault rocks plus elevated $\delta^{34}S$ indicate the involvement of mafic rocks in the hydrothermal system (Schmidt et al., 2007; Alt and Shanks, 2003). Pillow basalts in the area are hydrothermally altered to chlorite, quartz, albite and titanite, However, basalt alteration must be related to hydrothermal fluids upwelling from below, as sulfide mineralization and veins of quartz $\pm$ pyrite $\pm$ chalcopyrite are common in the basalts (Fig. 2). Metagabbro dikes are locally present in serpentinite, but the most likely reactive mafic component was a deeper-seated gabbroic intrusion providing heat to drive hydrothermal circulation and having much higher content of reactive sulfide relative to ultramafic rocks, as in ultramafic-hosted systems on the modern seafloor (Alt and Shanks, 2003; Petersen et al., 2009).

V. CONCLUSIONS

Normal faults in the ultramafic footwall are important components of oceanic detachments (Tucholke et al., 2008), providing pathways to feed volcanism at the surface, as well as for discharging hydrothermal fluids, but these faults remain poorly known on the modern seafloor. We document the first direct observations and sampling of such a fossil oceanic fault. Results can be useful to refine models for fluid flow in these faults, which depend on fault width, permeability contrasts, and transmissivity (Andersen et al., 2015). Upwelling high-temperature hydrothermal fluids in the fault zone resulted in replacement of serpentinite by talc + sulfide minerals. At the paleo-seafloor, the fault system evolved from discharge of high temperature (~350˚C) hydrothermal fluids, talc alteration, and formation of massive sulfide deposits, to carbonation of serpentinite at temperatures around 100˚C. Previous work has suggested that low temperature Lost City type venting can result from cooling of high-temperature hydrothermal fluids

(Foustoukos et al. (2008), but an important new result here is that such low-temperature venting and carbonation at the seafloor can evolve from higher-temperature black-smoker-type venting and massive sulfide formation.

ACKNOWLEDGMENTS

This project was supported by the National Science Foundation (NSF OCE-1536242 to JCA). We thank Dionysus Foustoukos and two anonymous reviewers for helpful comments.

REFERENCES

Abbate, E., Bortolotti V., Galbiati B. and Principi G., 1980, Carta geologica delle ofioliti del Bargonasco e dell'alta Val Graveglia. Scala 1:25.000. L.A.C. Firenze in: Bortolotti V. and Principi G., 2003, The Bargonasco-Upper Val Graveglia ophiolitic succession, northern Apennine, Italy. Ofioliti, 28, p. 137-140

Alt, J.C., and W.C. Shanks, 1998, Sulfur in serpentinized oceanic peridotites: Serpentinization processes and microbial sulfate reduction, Journal of Geophysical Research, 103, p. 9917–9929.

Alt, J.C., and Shanks, W.C., 2003. Serpentinization of abyssal peridotites from the MARK area, Mid-Atlantic Ridge: Sulfur geochemistry and reaction modeling, Geochimica et Cosmochimica Acta v. 67, p. 641-653.

Andersen, C., L. Rüpk , J. Hasenclever, I. Grevemeyer, S. Petersen, 2015. Fault geometry and permeability contrast control vent temperatures at the Logatchev 1 hydrothermal field, Mid-Atlantic Ridge, Geology v. 43, p. 51–54, doi:10.1130/G36113.1

Andreani, M., J. Escartin, A. Delacour, B. Ildefonse, M. Godard, J. Dyment, A. E. Fallick, and Y. Fouquet, 2014, Tectonic structure, lithology, and hydrothermal signature of the Rainbow massif (Mid-Atlantic Ridge 36˚14’N), Geochemistry Geophysics Geosystems,v. 15, doi:10.1002/2014GC005269.

Barrett, T.J., and Friedrichsen, H., 1989., Stable isotopic composition of atypical ophiolitic rocks from eastern Liguria, Italy. Chemical Geology,v. 80, p. 71-84.

Denny, A. R., Kelley, D. S., and Fruh-Green, G. L., 2015, Geologic evolution of the Lost City Hydrothermal Field, Geochemistry Geophysics Geosystems, v. 17, p. 375–394, doi:10.1002/2015GC005869.

Deschamps, F., Guillot, S., Godard, M., Chauvel, C., Andreani, M., Hattori, K., 2010. In situ characterization of serpentinites from forearc mantlewedges: timing of serpentinization and behavior of fluid-mobile elements in subduction zones. Chemical Geology v. 69, p. 262–277.

Douville, E., Charlou, J.L., Oelkers, E.H., Bienvenu, P., Jove Colon, C.F., Donval, J.P., Fouquet, Y., Prieour, D., and Appriou, P., 2002, The Rainbow vent fluids (36°14′N, MAR): the influence of ultramafic rocks and phase separation on trace metal content in Mid-Atlantic Ridge hydrothermal fluids. Chemical Geology, v. 184, p. 37–48.

Foustoukos, D.I., Davov, I.P., Janecky, D.R., 2008, Chemical and isotopic constraints on water/rock interactions at the Lost City hydrothermal field, 30˚N Mid-Atlantic Ridge. Geochimica et Cosmochimica Acta, v. 72, p. 5457-5474.

Foustoukos, D.I., Bizimis, M., Frisby, C., and Shirey, S.B., 2015, Redox controls on Ni–Fe–PGE mineralization and Re/Os fractionation during serpentinization of abyssal peridotite. Geochimica et Cosmochimica Acta v. 150, p. 11–25.

Frü -Green, G. L., Kelley, D. S., Bernasconi, S. M., Karson, J. A., Ludwig, K. A., Butterfield, D. A., Boschi, C. and Proskurowski, G., 2003, 30,000 Years of Hydrothermal Activity at the Lost City Vent Field. Science v. 301, p. 495–498.

Garuti, G., Alfonso, P., Proenza, J.A., and Zaccarini, F., 2009, Sulfur-Isotope Variations In Sulfide Minerals From Massive Sulfide Deposits of the Northern Apennine Ophiolites: Inorganic And Biogenic Constraints, Ofioliti, v. 34, p. 43-62

Garuti, G., Bartoli, O., Scacchetti, N., and Zaccarini, F., 2008, Geological setting and structural styles of Volcanic Massive Sulfide deposits in the northern Apennines (Italy): evidence for seafloor and sub-seafloor hydrothermal activity in unconventional ophiolites of the Mesozoic Tethys. Boletín de la Sociedad Geológica Mexicana v. 60, p. 121-145

Klein, F. and Garrido, C.J., 2011, Thermodynamic constraints on mineral carbonation of serpentinized peridotite, Lithos v. 126, p. 147–160

Malvoisin, B., 2015, Mass transfer in the oceanic lithosphere: Serpentinization is not isochemical, Earth and Planetary Science Letters v. 430, p. 75–85

Marroni, M., and Pandolfi, L., 2007, The architecture of an incipient oceanic basin: a tentative reconstruction of the Jurassic Liguria-Piemonte basin along the Northern Apennines–Alpine Corsica transect, International Journal of Earth Science v. 96, p. 1059–1078

McCaig A.M., Cliff, R.A., Escartin, J., Fallick, A.E., MacLeod, C.J., 2007, Oceanic detachment faults focus very large volumes of black smoker fluids, Geology, v. 35, p. 935–938.

McDonough, W.F. and Sun, S.S., 1995, The Composition of the Earth, Chemical Geology, v. 120, p. 223-253.

Niu, Y., 2004, Bulk-rock Major and Trace Element Compositions of Abyssal Peridotites: Implications for Mantle Melting, Melt Extraction and Post-melting Processes Beneath Mid-Ocean Ridges, Journal of Petrology, v. 45, p. 2423-2458.

Petersen, S., K. Kuhn, T. Kuhn, N. Augustin, R. Hékinian, L. Franz, and C. Borowski, 2009, The geological setting of the ultramafic-hosted Logatchev hydrothermal field (14°45′N, Mid-Atlantic Ridge) and its influence on massive sulfide formation, Lithos, doi:10.1016/j.lithos.2009.02.008

Principi G., Bortolotti V., Chiari M., Cortesogno L., Gaggero L.,Marcucci M., Saccani E. and Treves B.,, 2004, The pre-orogenic volcano-sedimentary covers of the Western Tethys Oceanic basin: A review. Ofioliti, 29, 177–211.

Rampone, E., Hofmann, A.W., and Razcek, I., 1998, Isotopic contrasts within the Internal Liguride ophiolite (N. Italy): the lack of a genetic mantle–crust link. Earth and Planetary Science Letters 163, p. 175–189

Rouxel, O., Fouquet, Y., and Ludden, J., 2004, Copper Isotope Systematics of the Lucky Strike, Rainbow, and Logatchev Sea-Floor Hydrothermal Fields on the Mid-Atlantic Ridge. Economic Geology v. 99, p. 585–600

Schmidt, K., A, Koschinsky, D. Garbe-Schoenberg, L. M. de Carvalho, R. Seifert, 2007, Geochemistry of hydrothermal fluids from the ultramafic-hosted Logatchev hydrothermal field, 15°N on the Mid-Atlantic Ridge: Temporal and spatial investigation, Chemical Geology v. 242, p. 1 –21

Tucholke, B.E., Behn, M.D., Buck, W.R., Lin, J., 2008. Role of melt supply in oceanic detachment faulting and formation of megamullions. Geology v. 36, p. 455–458.

Vasconcelos, C., McKenzie, J.A., Warthmann, R., Bernasconi, S.M., 2005, Calibration of the δ18O paleothermometer for dolomite precipitated in microbial cultures and natural environments. Geology v. 33, p. 317–320.

FIGURE CAPTIONS

Figure 1. Schematic of oceanic detachment fault exposing mantle material. Hydrothermal fluids driven by mafic intrusion can vent from the mafic hanging wall, or from the exposed ultramafic footwall via faulting at high angle to the detachment (See text).

Figure 2 A. Geological map around village of Reppia (redrawn from Abbate et al., 1980). Location shown on small inset. Seafloor faults indicated by dashed yellow lines. B. Google Earth image shows details of fault defined by reddish outcrops. Yellow diamonds, sulfide mineralization; white circles, background serpentinite sample locations. Ophiolitic breccia near area B consists mainly of Fe-Ti gabbro, to the SE of this it is mainly serpentinite/ophicalcite.

Figure 3. Chondrite normalized rare earth element diagram (McDonough and Sun, 1995). Solid lines, carbonated fault rocks; thin black lines, background serpentinite; dashed lines, talc fault rocks. Wide grey band is field for 3 fresh Ligurian peridotites

(Rampone et al., 1998). Seawater x 100 and hydrothermal fluid from the Rainbow seafloor ultramafic-hosted hydrothermal system from Douville et al. (2002).

Figure 4. Compositions of rocks normalized to average background serpentinite. All analyses recalculated volatile-free and plotted as $g/100cm^3$, using densities of 2.7 for talc fault rocks and for serpentinite (with trace magnetite), and 2.92 for carbonated fault rocks (intermediate between dolomite and ankerite).

Figure 5. A. Detail of seafloor normal fault in western portion of Fig 2. Fault juxtaposes hanging wall pillow basalt on the east (right) and serpentinite breccia on the west (left), and ends upward in massive sulfide, overlain by pelagic sediment. **D** Symbols as in Fig 2. B. Fe-dolomite (dol) and quartz (qz) in fault rock. C. Relict globular Cr-spinel.

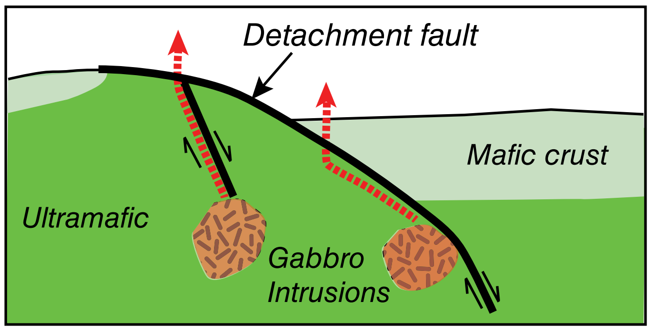

Figure 1. alt et al

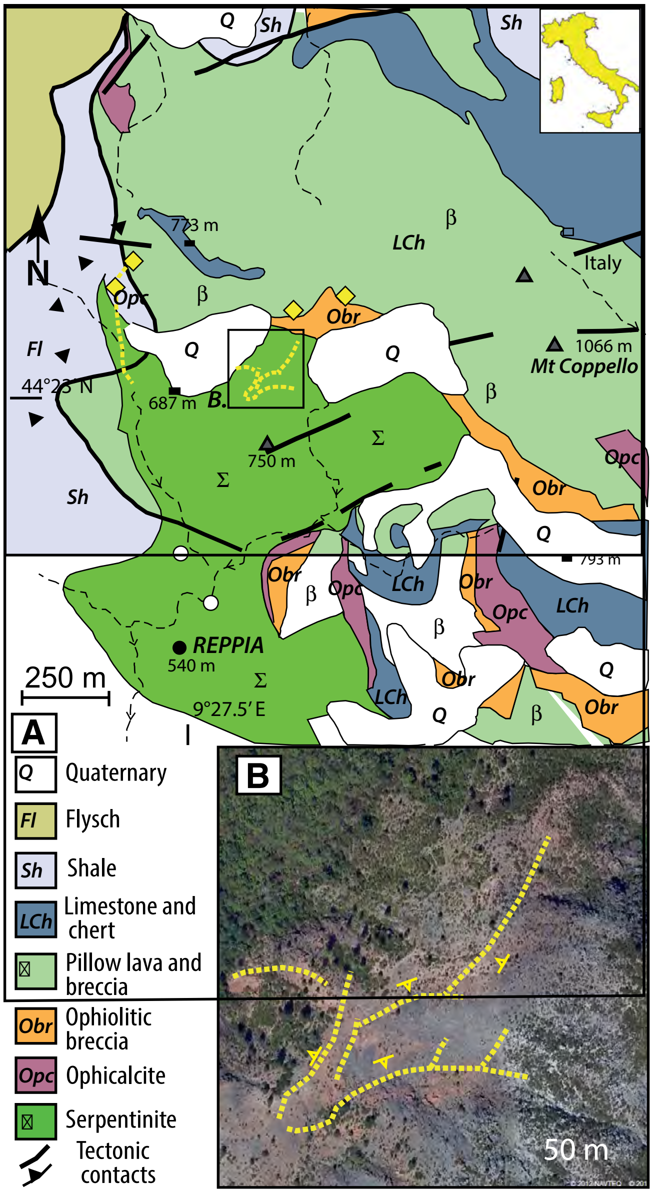

Figure 2. Alt et al

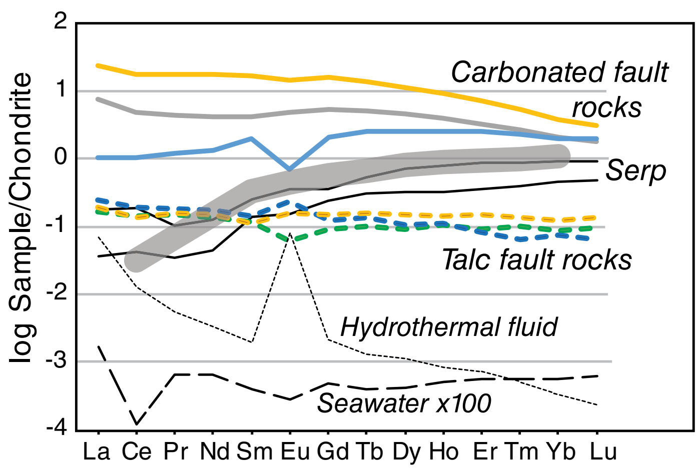

Figure 3. Alt et al

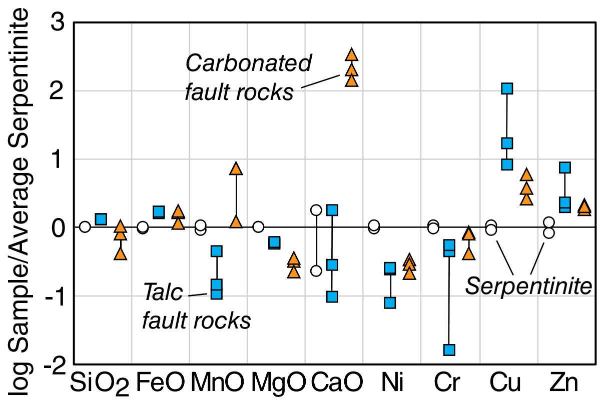

Figure 4 Alt et al

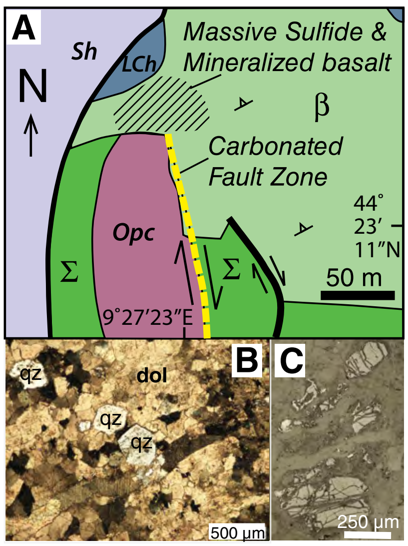

Figure 5. Alt et al

TABLE S3. REPRESENTATIVE ELECTRON MICROPROBE ANALYSES OF FE-DOLOMITE

Sample:	061509-1	061509-1	062612-14	062612-14
Latitude	44 23.194 N	44 23.194 N	44 23.193 N	44 23.193 N
Longitude	9 27.386 E	9 27.386 E	9 27.385 E	9 27.385 E
wt%				
$MgCO_3$	33.74	33.74	28.93	28.35
$CaCO_3$	46.24	46.29	47.31	45.50
$MnCO_3$	1.08	0.73	1.19	1.22
$FeCO_3$	19.94	19.27	24.22	26.64
$SrCO_3$	0.06	0.04	0.10	0.02
Total	101.06	100.07	101.75	101.73

TABLE S1. BULK ROCK CHEMISTRY

	Background Serpentinite		Carbonated Fault Rocks			Talc Fault Rocks		
SAMPLE	062712-12	91416-18	062612-14	061509-1	070914-2	062712-2	062612-22	062712-8
latitude	44˚ 22.670'N	44˚22.738'N	44 23.193 N	44 23.194 N	44˚ 23.167'N	44˚ 22.992'N	44˚ 23.066'N	44˚ 22.987'N
longitude	9˚ 27.589'E	9˚27.550'E	9 27.385 E	9 27.386 E	9˚ 27.383'E	9˚ 27.728'E	9˚ 27.771'E	9˚ 27.671'E
Altitude (m)	553	569	734	734	715	746	730	721
XRF wt%								
SiO2	38.32	38.05	23.31	11.08	31.29	55.20	54.95	54.51
TiO2	0.02	0.03	0.02	0.03	0.03	0.00	0.01	0.01
Al2O3	0.70	1.73	1.12	0.90	1.44	0.10	0.24	0.28
FeO*	8.21	7.73	9.90	6.25	10.73	13.89	14.70	14.25
MnO	0.11	0.10	0.58	0.52	0.10	0.05	0.01	0.02
MgO	38.69	37.16	9.40	5.84	10.83	24.36	23.67	24.36
CaO	0.04	0.29	24.76	37.93	18.28	0.32	0.05	0.02
Na2O	0.00	0.00	0.00	0.00	0.00	0.00	0.04	0.00
K2O	0.00	0.00	0.00	0.00	0.00	0.00	0.00	0.00
P2O5	0.00	0.00	0.01	0.01	0.00	0.00	0.00	0.00
LOI	12.67	13.44	29.26	33.97	26.35	5.93	5.18	5.78
Sum	98.75	98.52	98.36	96.53	99.05	99.86	98.85	99.23
CO_2 wt%			33.96	40.08				
$\delta^{13}C$ ‰ VPDB			-2.3	-1.8				
Normalized volatile-free								
SiO2	44.51	44.72	33.74	17.72	43.04	58.77	58.66	58.34
TiO2	0.02	0.03	0.03	0.05	0.05	0.00	0.01	0.01
Al2O3	0.81	2.03	1.62	1.43	1.98	0.11	0.25	0.29
FeO*	9.54	9.08	14.33	9.99	14.76	14.79	15.69	15.25
MnO	0.13	0.11	0.84	0.83	0.14	0.05	0.01	0.02
MgO	44.95	43.67	13.60	9.33	14.89	25.94	25.27	26.07
CaO	0.04	0.34	35.83	60.64	25.14	0.35	0.05	0.02
Na2O	0.00	0.00	0.00	0.00	0.00	0.00	0.04	0.00
K2O	0.00	0.00	0.00	0.00	0.00	0.00	0.00	0.00
P2O5	0.00	0.00	0.01	0.01	0.01	0.00	0.00	0.00
Total	100	100	100	100	100	100	100	100
MgO/SiO2	1.01	0.98	0.40	0.53	0.35	0.44	0.43	0.45

TABLE S1. BULK ROCK CHEMISTRY, Continued

	Background Serpentinite		Carbonated Fault Rocks			Talc Fault Rocks		
XRF (ppm)								
Ni	2538	2332	790	675	493	195	599	607
Cr	2051	2226	1716	1599	824	35	962	1171
V	26	42	54	26	45	4	20	22
Ga	1	2	3	2	5	2	2	0
Cu	18	21	108	48	68	158	1984	316
Zn	39	28	68	57	62	247	65	77
ICP-MS (ppm)								
La	0.01	0.04	1.77	5.56	0.25	0.06	0.04	0.04
Ce	0.03	0.12	2.96	10.66	0.65	0.12	0.09	0.08
Pr	0.00	0.01	0.41	1.61	0.11	0.02	0.01	0.01
Nd	0.02	0.06	1.95	8.15	0.60	0.08	0.06	0.07
Sm	0.02	0.04	0.63	2.52	0.29	0.02	0.02	0.02
Eu	0.01	0.02	0.28	0.82	0.04	0.01	0.00	0.01
Gd	0.05	0.07	1.09	3.19	0.42	0.02	0.02	0.03
Tb	0.01	0.02	0.18	0.50	0.09	0.00	0.00	0.01
Dy	0.08	0.18	1.12	2.83	0.64	0.03	0.02	0.04
Ho	0.02	0.04	0.21	0.50	0.14	0.01	0.01	0.01
Er	0.06	0.14	0.53	1.14	0.40	0.01	0.01	0.02
Tm	0.01	0.02	0.06	0.13	0.06	0.00	0.00	0.00
Yb	0.07	0.14	0.33	0.61	0.32	0.01	0.01	0.02
Lu	0.01	0.02	0.04	0.07	0.05	0.00	0.00	0.00
Ba	0	0	6	7	3	1	0	1
Th	0.00	0.02	0.03	0.03	0.02	0.02	0.02	0.01
Nb	0.01	0.01	0.04	0.05	0.09	0.02	0.03	0.02
Y	0.49	1.05	7.28	14.92	3.38	0.15	0.10	0.20
Hf	0.02	0.03	0.02	0.05	0.05	0.00	0.02	0.01
Ta	0.00	0.00	0.02	0.02	0.01	0.00	0.00	0.00
U	0.00	0.01	0.19	0.07	0.28	0.01	0.00	0.00
Pb	0.14	0.60	0.07	0.01	0.23	4.32	0.81	0.39
Rb	0.1	0.0	0.1	0.1	0.1	0.2	0.1	0.1
Cs	0.01	0.00	0.09	0.05	0.08	0.04	0.02	0.11
Sr	1	1	263	612	113	1	1	1
Sc	8.5	11.1	4.5	5.1	6.2	0.2	3.7	1.3
Zr	0	1	1	2	2	0	1	0

*total Fe as FeO

Bulk rock major and trace elements were analyzed by X-ray fluorescence and ICP-MS at Washington State University. Results for major elements, Ni, Cu, Th, Hf, Sr, Sc, Cs, Zr, and Y, are within 5% of accepted standard values, and Cu, Zn, Pb, Nb, Ba and U are reproducible within 10%. Total Carbon contents and isotope compositions of bulk rocks were determined using a Costech Element Analyzer coupled to a Thermo Scientific Delta V plus mass spectrometer. Carbon contents are reproducible ±70 ppm and δ13C values are ±0.5‰. Oxygen and carbon isotopes of micro-drilled carbonate were analyzed on a Finnigan Mat 251 mass spectrometer coupled to a Finnigan Kiel automated preparation device. Standards are reproducible within 0.1‰ for both. Separated sulfide minerals were combusted to SO2 using a Flash 2000 elemental analyzer and introduced into a Thermofinnigan Delta XP mass spectrometer for measurement of 34S/32S ratios. Standards were reproducible to ±0.2‰.

TABLE S2. MINERAL STABLE ISOTOPE DATA

Sample	Latitude	Longitude	Mineral	$\delta^{13}C$ (‰VPDB)	$\delta^{18}O$ (‰VSMOW)	$\delta^{34}S$ (‰VCDT)
62612-14	44 23.1931 N	9 27.3849 E	euhedral Fe Dolomite	-0.8	20.9	
62612-14	44 23.1931 N	9 27.3849 E	feathery Fe-dolomite	-1.5	20.2	
61509-1	44 23.1937 N	9 27.3862 E	feathery Fe-dolomite	-0.8	19.8	
62712-10	44 22.9698 N	9 27.664 E	pyrite			5.7

TABLE S3. REPRESENTATIVE ELECTRON MICROPROBE ANALYSES OF FE-DOLOMITE

Sample:	061509-1	061509-1	062612-14	062612-14
Latitude	44 23.194 N	44 23.194 N	44 23.193 N	44 23.193 N
Longitude	9 27.386 E	9 27.386 E	9 27.385 E	9 27.385 E
wt%				
$MgCO_3$	33.74	33.74	28.93	28.35
$CaCO_3$	46.24	46.29	47.31	45.50
$MnCO_3$	1.08	0.73	1.19	1.22
$FeCO_3$	19.94	19.27	24.22	26.64
$SrCO_3$	0.06	0.04	0.10	0.02
Total	101.06	100.07	101.75	101.73